Supplemental Material

Anomalous thermal conductivity in 2D silica nanocages of immobilizing noble gas atom

Yang Wang,[1] Zhibin Gao,[1, †] Xiaoying Wang,[1] Jinping Sun,[2] Minxuan Feng,[1]
Yuzhou Hao, [1]Xuejie Li, [1] Yinchang Zhao[3, *], Xiangdong Ding[1]

[1] State Key Laboratory for Mechanical Behavior of Materials, School of Materials Science and Engineering, Xi'an Jiaotong University, Xi'an 710049, China

[2] School of Materials Science and Engineering, Harbin Institute of Technology at Weihai, 2 West Wenhua Road, Weihai 264209, China

[3] Department of Physics, Yantai University, Yantai 264005, China

Authors to whom correspondence should be addressed: zhibin.gao@xjtu.edu.cn [†]; y.zhao@ytu.edu.cn[*]

When dealing with the solution of the phonon Boltzmann Transport Equation (BTE) [1], the lattice thermal conductivity κ_L can be computed as,

$$\kappa_L = \frac{\hbar^2}{k_B T^2 V N_0} \sum_\lambda n_\lambda (n_\lambda + 1) \omega_\lambda^2 \, \nu_\lambda \otimes \nu_\lambda \tau_\lambda \qquad (S1)$$

where $\hbar$, T, k_B, V, N_0 are the reduced Planck's constant, absolute temperature, Boltzmann constant, original unit cell volume, and the total number of phonon wavevectors sampled in the first Brillouin zone, respectively. n_λ, ω_λ, ν_λ, and τ_λ are the equilibrium components of the phonon population, frequency, group velocity, and lifetime for the λ mode (wave vector q and branch index s), respectively. Except τ_λ, all the parameters mentioned above can be obtained from harmonic approximation (HA). Typically, τ_λ can be derived from perturbation theory considering three-phonon scattering [2, 3]. Temperature-dependent phonon dispersions can be accounted for by the anharmonic phonon renormalization (APRN) at finite temperatures [4-9]. Among various existing methods, SCPH [10, 11] approximation is an effective approach that rigorously explains the first-order corrections of the fourth-order anharmonicity to phonon frequencies. It can provide a better description of soft phonon modes and strong anharmonicity. In brief, in the SCPH approximation, the temperature-dependent renormalized phonon frequency Ω_λ can be obtained through the following equation

$$\Omega_\lambda^2 = \omega_\lambda^2 + 2\Omega_\lambda \sum_{\lambda_1} I_{\lambda\lambda_1} \qquad (S2)$$

where ω_λ is the original phonon frequency from the harmonic approximation. The scalar $I_{\lambda\lambda_1}$ can be obtained as,

$$I_{\lambda\lambda_1} = \frac{\hbar}{8N_0} \frac{V^{(4)}(\lambda, -\lambda, \lambda_1, -\lambda_1)}{\Omega_\lambda \Omega_{\lambda_1}} \left[1 + 2n_\lambda(\Omega_{\lambda_1})\right] \qquad (S3)$$

in which $V^{(4)}$ is the fourth-order IFCs in the reciprocal representation. The phonon population

n_λ satisfies Bose-Einstein distribution as a function of temperature. Both Eq. (S2) and Eq. (S3) have parameters $I_{\lambda\lambda_1}$ and Ω_λ in common, and thus the SCPH equation can be solved iteratively. Note that $I_{\lambda\lambda_1}$ can be interpreted as the interaction between a pair of phonon modes, λ and λ_1 including the temperature effects [10, 11].

SCP calculations were executed using the ALAMODE package. Since a 3 × 3 × 1 supercell was used to generate IFCs, a fixed 3 × 3 × 1 q-grid was employed for real-space Fourier interpolation. For all temperatures considered, a mixing parameter of 0.1 was used in the SCP iteration.

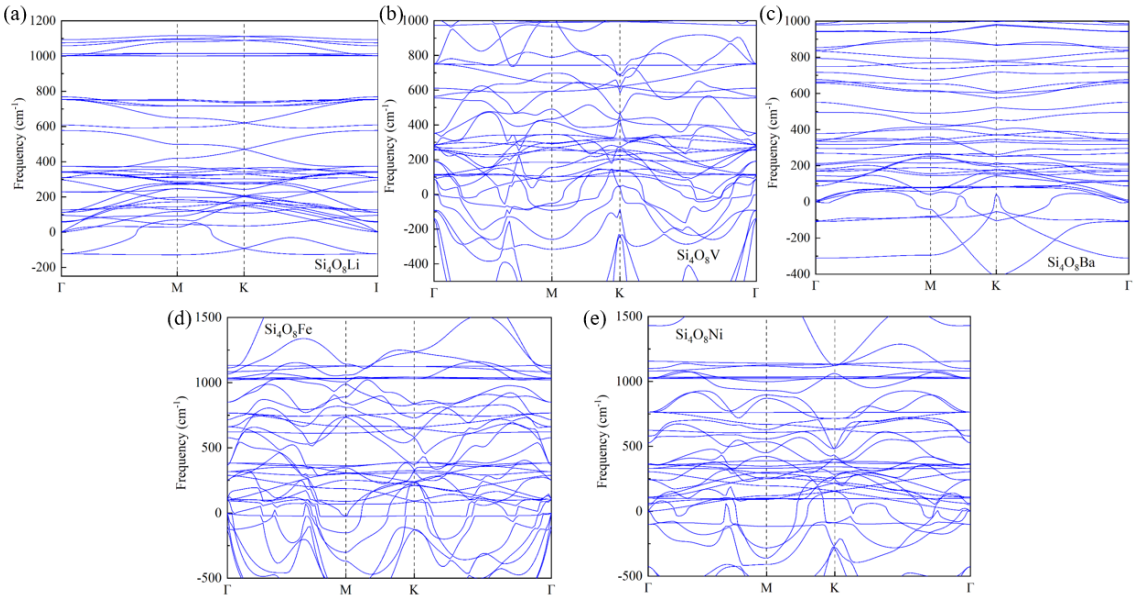

FIG. S1. (a)-(e) The phonon dispersions for Si_4O_8Li, Si_4O_8V, Si_4O_8Ba, Si_4O_8Fe, and Si_4O_8Ni. It exhibits imaginary frequencies in the harmonic approximation (HA) phonon spectra, indicating the dynamic instability of this structure. The large electronegativity difference between the guest atom and the host framework could lead to structural instability since excess dopant electrons will cause a substantial increase in energy and subsequent collapse of the nanocage.

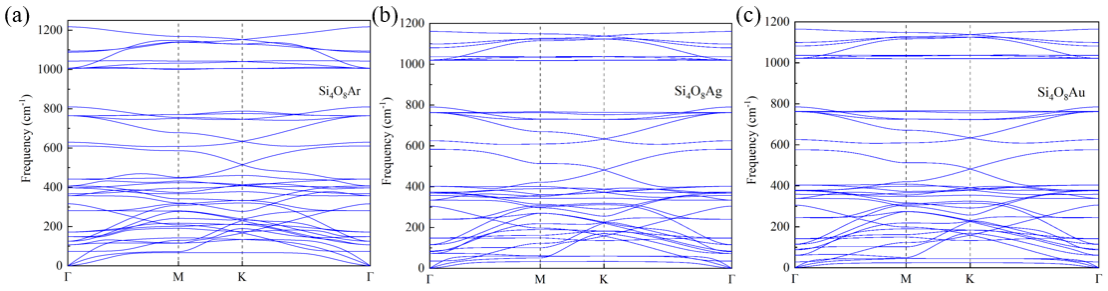

FIG. S2. (a)-(c) The phonon dispersions for Si_4O_8Ar, Si_4O_8Ag and Si_4O_8Au. It does not exhibit imaginary frequencies in the HA phonon spectra, indicating the dynamic stability of these structures. A stable host-guest system can be formed when the electronegativity of the guest atom, closely aligns with the electronegativity of the host framework.

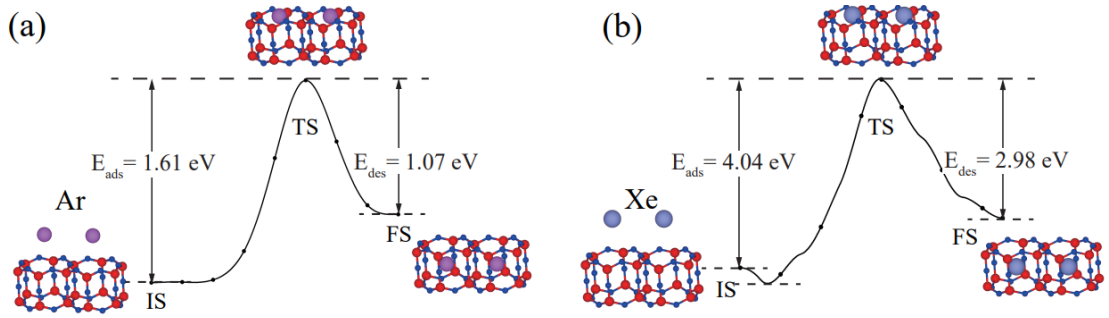

FIG. S3. (a)-(b) The minimum energy path for doped atoms as obtained climbing image nudged elastic band calculations (CI-NEB) [12], considering the trapping of Ar and Xe atoms. E_{ads} and E_{des} represent the activation energies for adsorption and desorption, respectively.

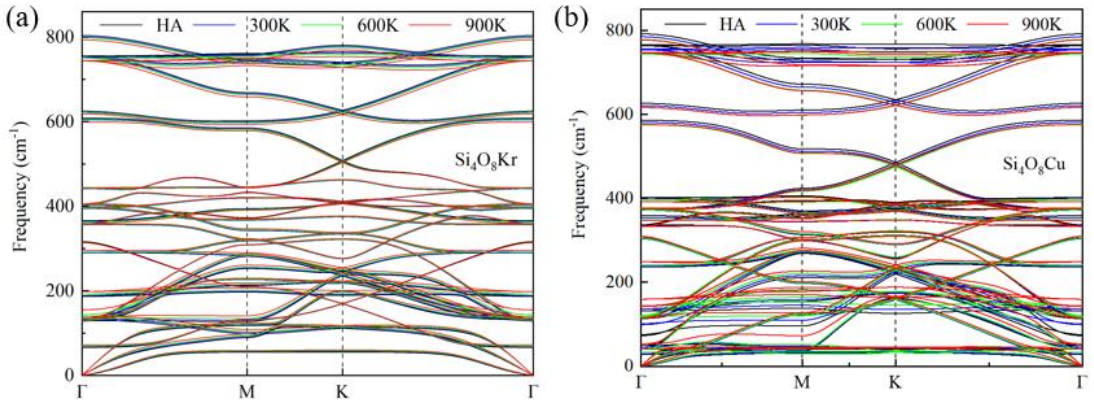

FIG. S4. (a)-(b) The renormalized phonon dispersion of Si_4O_8Kr and Si_4O_8Cu at different temperatures. HA is the phonon spectrum from harmonic approximation. It exhibits stability at both low and high temperatures. Under the influence of temperature effects, the phonon branches of the Si_4O_8Kr and Si_4O_8Cu phonon spectrum show a hardening phenomenon.

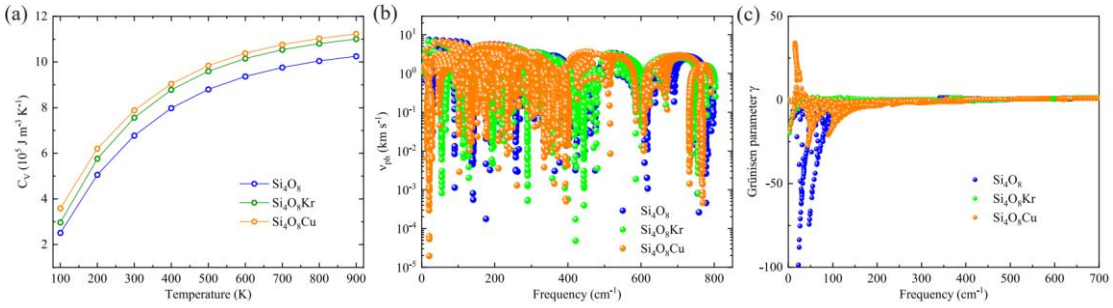

FIG. S5. (a) Heat capacity C_V as a function of temperature. (b) Phonon group velocity v_{ph} at 300 K. (c) Grünisen parameter. The blue, green, and orange colors represent Si_4O_8, Si_4O_8Kr, and Si_4O_8Cu, respectively.

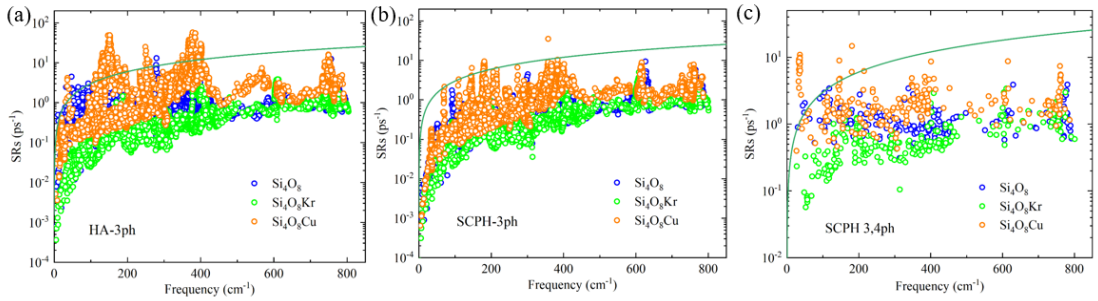

FIG. S6. (a)-(c) Calculated phonon scattering rates compared with Si_4O_8, Si_4O_8Kr, and Si_4O_8Cu for HA of 3ph, SCPH of 3ph, SCPH of 3ph and 4ph at 300 K, respectively. We observed contrasting trends in the scattering rates of Si_4O_8Kr, and Si_4O_8Cu. Doping with Kr atoms leads to a decrease in scattering rates while doping with Cu atoms increases scattering rates. The fluctuation in scattering rates aligns with the observed trends in thermal conductivity variations.

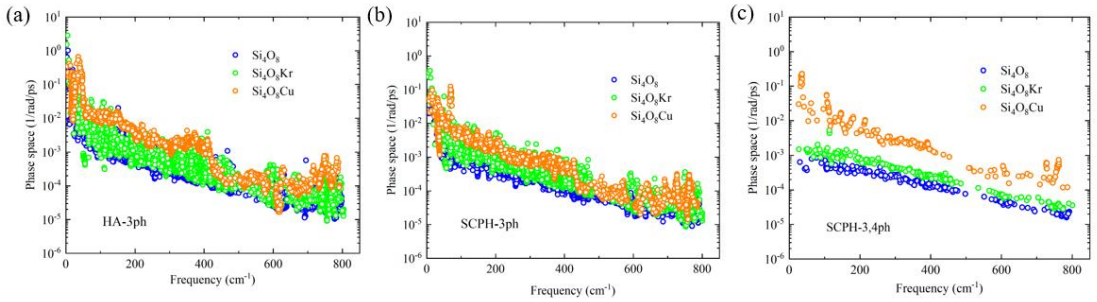

FIG. S7. (a)-(c) Calculated phase space compared Si_4O_8, Si_4O_8Kr, and Si_4O_8Cu for the HA of 3ph, SCPH of 3ph, SCPH of 3ph and 4ph phase at 300 K, respectively. We observed the same trends in the phase space of Si4O8Kr, and Si4O8Cu. Doping with Kr and Cu atoms leads to an increase in phase space. The indication is that the scattering from the dopant atoms has a significant impact on the scattering phase space, with the influence of Kr atoms being greater than that of lattice distortion.

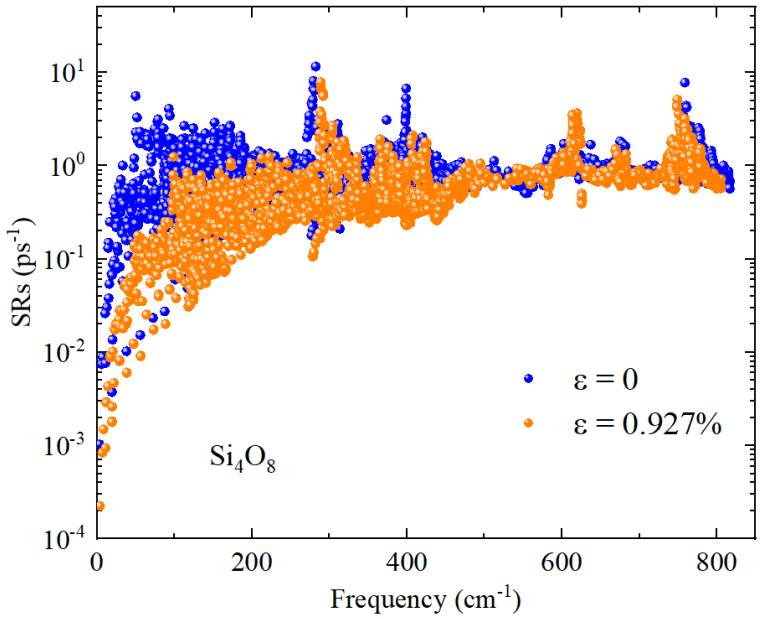

FIG. S8. Calculated phonon scattering rates compared with Si_4O_8 without strain and ε =0.927% strain for HA of 3ph at 300 K, respectively. Strain leads to a decrease in scattering rates, thereby increasing the lattice thermal conductivity. The fluctuation in scattering rates aligns with the observed trends in thermal conductivity variations.

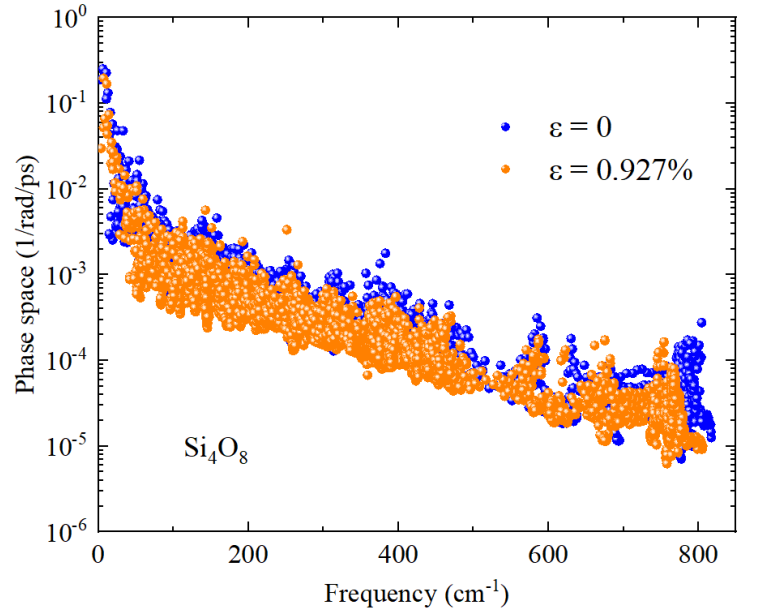

FIG. S9. Calculated phase space compared with Si_4O_8 without strain and ε = 0.927% strain for HA of 3ph at 300 K, respectively. Strain leads to a decrease in phase space. The fluctuation in scattering rates aligns with the observed trends in thermal conductivity variations.

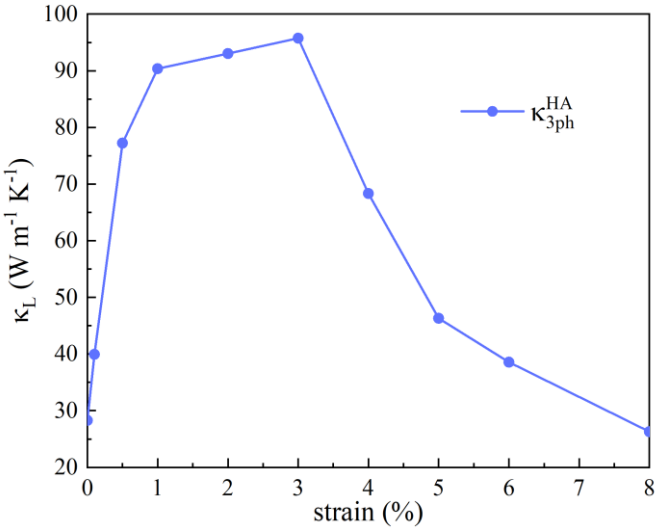

FIG. S10. Lattice thermal conductivity κ_L of 2D silica with applied tensile strain at 300 K.

References:

[1] W. Li, J. Carrete, N. A. Katcho, and N. Mingo, Comput. Phys. Commun. 185, 1747 (2014).
[2] A. Debernardi, S. Baroni, and E. Molinari, Phys. Rev. Lett. 75, 1819 (1995).
[3] Z. Gao, F. Tao, and J. Ren, Nanoscale 10, 12997 (2018).
[4] N. Li, B. Li, and S. Flach, Phys. Rev. Lett. 105, 054102 (2010).
[5] P. Souvatzis, O. Eriksson, M. I. Katsnelson, and S. P. Rudin, Phys. Rev. Lett. 100, 095901 (2008).
[6] I. Errea, B. Rousseau, and A. Bergara, Phys. Rev. Lett. 106, 165501 (2011).
[7] I. Errea, M. Calandra, and F. Mauri, Phys. Rev. B 89, 064302 (2014).
[8] Y. Xia, Appl. Phys. Lett. 113, 073901 (2018).
[9] N. K. Ravichandran and D. Broido, Phys. Rev. X 10, 021063 (2020).
[10] T. Tadano and S. Tsuneyuki, Phys. Rev. B 92, 054301 (2015).
[11] Y. Xia, V. I. Hegde, K. Pal, X. Hua, D. Gaines, S. Patel, J. He, M. Aykol, and C. Wolverton, Phys. Rev. X 10, 041029 (2020).
[12] Henkelman, G.; Uberuaga, B. P.; Jónsson, H. J. Chem. Phys.113, 9901–9904 (2000).